Title

The cold-inducible RNA-binding protein RBM3 stabilises viral mRNA at cooler temperatures representative of the upper respiratory tract.

Authors

Hannah L Coutts[1], Hannah L Turkington[1], Swathi Sukumar[1], Stefano Bonazza[1], Emily Peate[1], Erin M P E Getty[1], Ultan F Power[1], David G Courtney[1]

Affiliations

1 Wellcome-Wolfson Institute for Experimental Medicine, Queen's University Belfast, Belfast BT9 7BL, UK

Abstract

Temperature is a critical determinant of host–pathogen interactions in the respiratory tract, where influenza A virus (IAV) has adapted to the cooler environment of the upper respiratory tract (URT) to enable efficient replication and transmission. The cold-inducible RNA-binding protein RBM3 is highly expressed in nasopharyngeal tissue and is known to stabilise mRNAs under hypothermic conditions; however, its role during viral infection has not been defined.

Here, we identify RBM3 as a key host factor that facilitates IAV replication at sub-physiological temperatures. siRNA-mediated depletion of RBM3 significantly impaired viral replication, while its constitutive overexpression at 37°C restored replication to levels typically observed at 33°C. Mechanistically, RBM3 binds directly to viral nucleoprotein (NP) mRNA, prolongs its half-life, and promotes the formation of cytoplasmic ribonucleoprotein granules. This effect was abolished in an RNA-binding-deficient RBM3 mutant, confirming the requirement for direct RNA interaction. Crucially, this positive regulation of NP mRNA was validated in well-differentiated primary nasal epithelial cells, highlighting the physiological relevance of RBM3 in the human URT.

These results reveal a temperature-sensitive host–virus interaction that promotes IAV replication in the cooler URT, a key site for viral shedding and transmission. By linking environmental temperature, host RNA-binding proteins, and viral mRNA stability, this study uncovers a novel mechanism of respiratory virus adaptation and identifies RBM3 as a potential therapeutic target for limiting early-stage viral replication and transmission.

Author Summary

To establish productive infection and ensure transmission, respiratory viruses such as influenza A virus (IAV) must adapt to the diverse environments of the human respiratory tract. One key challenge is the temperature gradient that exists between the upper and lower respiratory tract. The upper respiratory tract (URT), the main site of viral entry and transmission, maintains a lower physiological temperature (~33°C) than the lower respiratory tract (~37°C), creating a distinct cellular environment. In this study, we investigated how this cooler URT temperature alters the landscape of RNA-binding proteins (RBPs), which play a central role in regulating gene expression after transcription. Using mass spectrometry-based profiling and molecular virology approaches, we identified a cold-inducible RBP, RBM3, as significantly enriched at 33°C and acting as a key host factor during IAV infection. We show that RBM3 binds directly to viral nucleoprotein (NP) mRNA, promoting its stability and forming cytoplasmic granules that enhance the production of infectious virions. Importantly, disrupting RBM3's RNA-binding ability abolished this proviral effect. These findings reveal that RBM3, elevated in the cooler URT environment, directly supports IAV replication. This work highlights how subtle physiological differences in host tissue can reshape post-transcriptional regulation and influence the outcome of respiratory virus infection.

52 ## Introduction

53 Respiratory viruses remain an ever-present pandemic concern, in part due to their efficient
54 airborne mode of transmission [1]. While severe pathology from respiratory viruses such as
55 influenza A virus (IAV) or SARS-CoV-2 is typically associated with replication in the lower
56 respiratory tract (LRT), transmission predominantly occurs via small droplets and aerosols
57 expelled from the upper respiratory tract (URT) [1–4]. Thus, advancing research into the
58 unique cellular environment of the nasopharyngeal epithelium is critical to deepening our
59 understanding of respiratory virus transmission [5] and will ultimately support public health
60 efforts to develop the next generation of nasal vaccines that boost mucosal immunity [6,7].

61 A key feature of this URT environment is its lower physiological temperature, with
62 nasopharyngeal epithelial cells typically residing at or below 33°C—several degrees cooler
63 than the average core body temperature of 37°C [8]. Though seemingly minor, this
64 temperature difference has far-reaching effects on cellular processes, including viral
65 replication kinetics [9]. Because molecular interactions and reaction rates are governed by
66 thermodynamic principles, temperature is a fundamental variable in regulating biochemical
67 activity. Accordingly, the interaction landscape—including RNA and protein folding, stability,
68 and binding—is substantially altered under cooler conditions [10]. These changes can lead to
69 RNA or protein misfolding [10–12], and, crucially, to temperature-sensitive differences in
70 RNA-binding protein (RBP) affinities for target RNAs, with wide-ranging effects on post-
71 transcriptional regulation [13].

72 Temperature-dependent variation in RBP–RNA binding has significant implications for mRNA
73 spatial localisation, stability, and translation, processes that can influence viral RNA
74 processing and immune evasion [14]. While prior studies have observed temperature-driven

75 changes in transcript and protein abundance [15,16], it remains poorly understood how
76 growth temperature alters the global landscape of RBPs that bind to cellular mRNAs—
77 collectively known as the RBPome.

78 The central aim of this study was to characterise the post-transcriptional environment
79 encountered by respiratory viruses, with a focus on IAV, and to determine how altered growth
80 temperature affects viral mRNA regulation. Specifically, we profiled the mRNA-bound
81 RBPome of lung epithelial cells (A549 cells) grown at 37°C and 33°C, mimicking LRT and URT
82 temperatures, respectively. Recent studies have highlighted the critical role of the host
83 RBPome in shaping viral replication by regulating nuclear export [17], translation [18], and
84 genome replication [19], underscoring the importance of this approach [18,20].

85 Our data reveal extensive temperature-dependent variation in RBPs associated with cellular
86 mRNAs, identifying large sets of RBPs whose binding is either enriched or depleted at 33°C
87 relative to 37°C. Among the most striking findings was the cold-induced enrichment of RNA
88 Binding Motif 3 (RBM3), a well-characterised cold-shock protein known to support cell
89 survival under hypothermic stress [21,22]. Notably, RBM3 was recently identified by our
90 group in an IAV mRNA interactome screen [23]. Here, we build on that work and demonstrate
91 that RBM3, by stabilising viral transcripts, acts as a pro-viral host factor during IAV infection
92 in A549 cells.

93 Crucially, we validate these findings in well-differentiated primary nasal epithelial cells
94 (PNECs) derived from multiple human donors. Using antisense oligonucleotide (ASO)-
95 mediated induction of RBM3 expression [24] followed by infection, we show that elevated
96 RBM3 enhances IAV replication in this physiologically relevant URT model.

97 Together, these findings reveal that RNA regulation in the URT occurs within a distinct post-
98 transcriptional landscape, shaped by cooler tissue temperature. This environment profoundly
99 impacts viral replication dynamics and represents a key barrier that respiratory viruses, such
100 as IAV, have overcome to establish infection and achieve transmission. Understanding these
101 adaptations not only provides new insights into viral evolution and host–pathogen
102 interactions but also offers a foundation for developing temperature-sensitive antiviral
103 strategies and next-generation respiratory vaccines.

104 **Results**

105 The cold RBPome of A549 cells reveals RBM3 as a significantly enriched mRNA interactor

106 As previously mentioned, the temperature gradient normally observed in the respiratory tract
107 is known to yield distinct variations in cellular transcriptomes and proteomes [15,16] (Figure
108 1A). To identify specific RBPs that are differentially regulated through temperature, we
109 employed RNA Interactome Capture (RIC) [25] on A549 cells incubated for 48 h at 33°C or
110 37°C. This method allowed for the purification and identification of poly(A) RNA-binding RBPs
111 via UV crosslinking and mass spectrometry (Figure 1B). Quality control of the protein samples
112 to be analysed by MS was assayed by silver staining, highlighting the presence of distinct
113 protein compositions between experimental conditions (Figure 1C). We observed clear
114 differences in band patterns between the 33°C and 37°C in the pulldown samples indicative
115 of the differences between the two proteomes, which were evaluated by LC-MS/MS. The
116 resulting dataset was analysed for enrichment of RBPs in the 33°C compared to the 37°C
117 samples (Figure 1D). Adjusted P values were calculated with a cutoff of $p<0.05$. Between these
118 datasets, we identified a considerable number of RBPs that were preferentially enriched in
119 either temperature. Interestingly, a total of 209 RBPs were shared between 33°C and 37°C
120 (Figure 1E and 1F). Of the total 423 RBPs identified across all datasets, 296 were found to be
121 significantly regulated by alterations in growth temperature. Those that were present in both
122 datasets, but significantly enriched at 33°C, included RBM3, YBOX1, HNRNPC, RBM47 and
123 SND1 (Supplementary Table 1 and 2). Overall, these datasets are important evidence that the
124 RBP environment of the cell is very plastic. Several factors are selectively overrepresented at
125 cold temperatures and thus could play a role in respiratory virus infections.

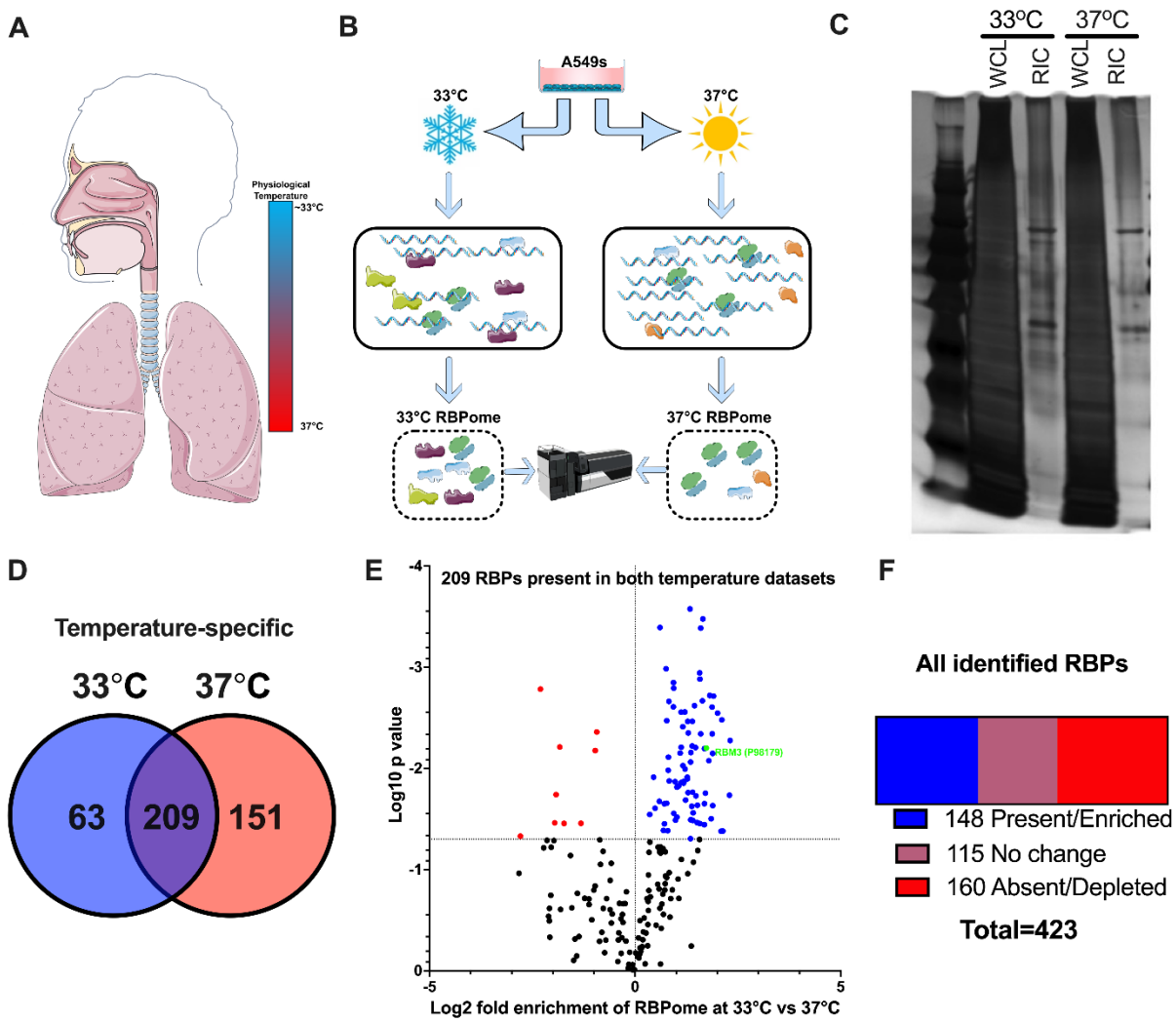

Figure 1 – Cooler growth temperatures vastly alter the RBPome of A549 cells.

(A) *Schematic representation of the temperature gradient between the URT and LRT.* ***(B)*** *Schematic of the workflow for RIC in A549 cells incubated at 33°C or 37°C.* ***(C)*** *Representative silver stain of a gel with the RIC whole cell lysate input (WCL) and pulldown (RIC) samples from protein populations at 33°C and 37°C.* ***(D)*** *Venn diagram showing RBPs present in either 33°C datasets, 37°C datasets or both.* ***(E)*** *Volcano plot showing the enrichment of RBPs isolated from A549 33°C and 37°C pulldown samples.* ***(F)*** *Representation of the proteins significantly altered between datasets, whether by presence/absence or enrichment/depletion. Datasets derived from 3 independent biological samples.*

RBM3 is a positive regulator of IAV replication in A549s, mediated by its RNA-binding activity

One of the top hits enriched in the 33°C dataset was RBM3. This cold-inducible protein was recently identified by us and our colleagues when performing an IAV A/WSN/33 NP mRNA interactome screen [23], and therefore presented an attractive option as an RBP that could play a role in IAV replication in the URT. Firstly, to investigate whether RBM3 impacts IAV replication we performed siRNA-mediated knockdown of RBM3 in A549 cells, followed by infection by WSN at an MOI 0.01 for 48 h. qPCR analysis confirmed effective knockdown with

141 a >95% decrease in RBM3 mRNA levels compared to a nonspecific control siRNA (NSC) (Figure
142 2A). Total RNA was harvested at 0, 8, 24 and 48 hours post infection (hpi), and levels of viral
143 mRNA were analysed via qPCR. Overall, depletion of RBM3 resulted in a significant decrease
144 in viral HA, NA, NP and M2 mRNA at 24 and 48 hpi (Figure 2B and Supp Figure 1). Most notably,
145 we observed a nearly four-fold decrease in levels of NP mRNA at 24 hpi (Figure 2B). Not
146 surprisingly, this negative impact on viral transcript levels translated through to virus
147 production, resulting in a significant drop in viral titres below the level of detection (Figure
148 2C).

149 Recent work shows HNRNPH1 controls RBM3 via poison-exon splicing: inclusion of exon 3a in
150 RBM3 pre-mRNA triggers NMD [25], and weak HNRNPH1 binding at 37 °C permits exon
151 inclusion (low RBM3), whereas stronger binding at 30–33 °C excludes exon 3a, boosting RBM3
152 levels [13]. In A549s transfected with siNSC or siH1 for 48 h and then treated ±CHX for 16 h,
153 RT–PCR spanning exons 3–4 revealed exon 3a only in siH1+CHX samples (Supp Fig 2A), and
154 qPCR showed an ~11-fold greater inclusion versus siH1+DMSO (Supp Fig 2B). siH1 also
155 reduced RBM3 mRNA (Supp Fig 2C). After WSN infection (MOI 0.01), siH1 cells had
156 significantly lower NP mRNA at 0–48 hpi (Supp Fig 2D) and reduced viral titres (Supp Fig 2E).
157 Thus, HNRNPH1 modulates RBM3 expression by poison-exon regulation, affecting IAV
158 replication.

159 On identifying RBM3 as a potentially important RBP during IAV replication, we sought to
160 determine whether this pro-viral phenotype arises from a direct interaction between RBM3
161 and viral RNA. However, as evidenced from the RIC MS, the cold environment affects the host
162 globally, and it would be difficult to ascertain the effect of RBM3 alone on viral replication at
163 33°C. To circumvent this limitation, a cell line expressing cold-induced levels of RBM3 at 37°C
164 was needed. First, a panel of cell lines commonly used to study respiratory viruses was

165 assessed to determine their cold responsiveness, quantified by their ability to induce RBM3
166 when cultured at 33°C for 48 h. Primary nasal epithelial cells (PNECs) were used as a positive
167 control as it was expected that these would be highly responsive to cooler growth
168 temperatures. RNA was extracted and the levels of RBM3 expression were quantified by
169 qPCR, normalised to the levels observed with culturing at 37°C for each cell type (Figure 2D).
170 While PNECs were the greatest responders, with an approximate 7-fold increase in RBM3
171 mRNA levels, A549s and 293Ts both demonstrated a >3-fold increase in RBM3 levels.
172 Considering that immortalised cells can be manipulated to a greater extent that PNECs, we
173 proceeded to use A549s to develop greater mechanistic insights into the role of RBM3 during
174 IAV infection. A lentivirus-mediated stably overexpressing RBM3-Flag, clonal A549 cells line,
175 termed A549-RBM3+, was established that could be cultured at 37°C. Upon quantification by
176 qPCR, RBM3 levels were found to be >3-fold increased over an empty vector control line
177 (Figure 2E), mimicking the levels seen upon culturing of parental A549s at 33°C. Viral
178 production was then quantified in these A549-RBM3+ cells, with RBM3 overexpression
179 inducing a significant increase in viral titres of >3.5-fold (Figure 2F).

180 RBM3 is composed of two major domains; an RNA Recognition Motif (RRM) found at the C-
181 terminus, and an N-terminus arginine-glycine rich (RGG) domain (Figure 2G) [26]. The former
182 contains two highly conserved RNA binding regions, RNP2 and RNP1. After establishing the
183 binding between NP mRNA and RBM3, we proceeded to investigate how an RNA-binding null
184 mutant RBM3 would affect viral replication. We hypothesised that any pro-viral function
185 would be lost through ablation of RNA-binding. To test this, we created an RBM3 RNA-binding
186 null mutant cell-line, in which mutations were introduced to substitute phenylalanine (F)
187 residues within RNP2 and RNP1 to leucine (L) (Figure 2G). Previous studies have shown that
188 single L>F substitutions within RNP motifs disrupt the RNA binding ability [27]. When viral

189 titres from infected A549-RBM3+ and A549-RBM3 mutant cell lines were compared (Figure

190 2H), we observed a significant >95% decrease in titres from the RBM3 mutant cells.

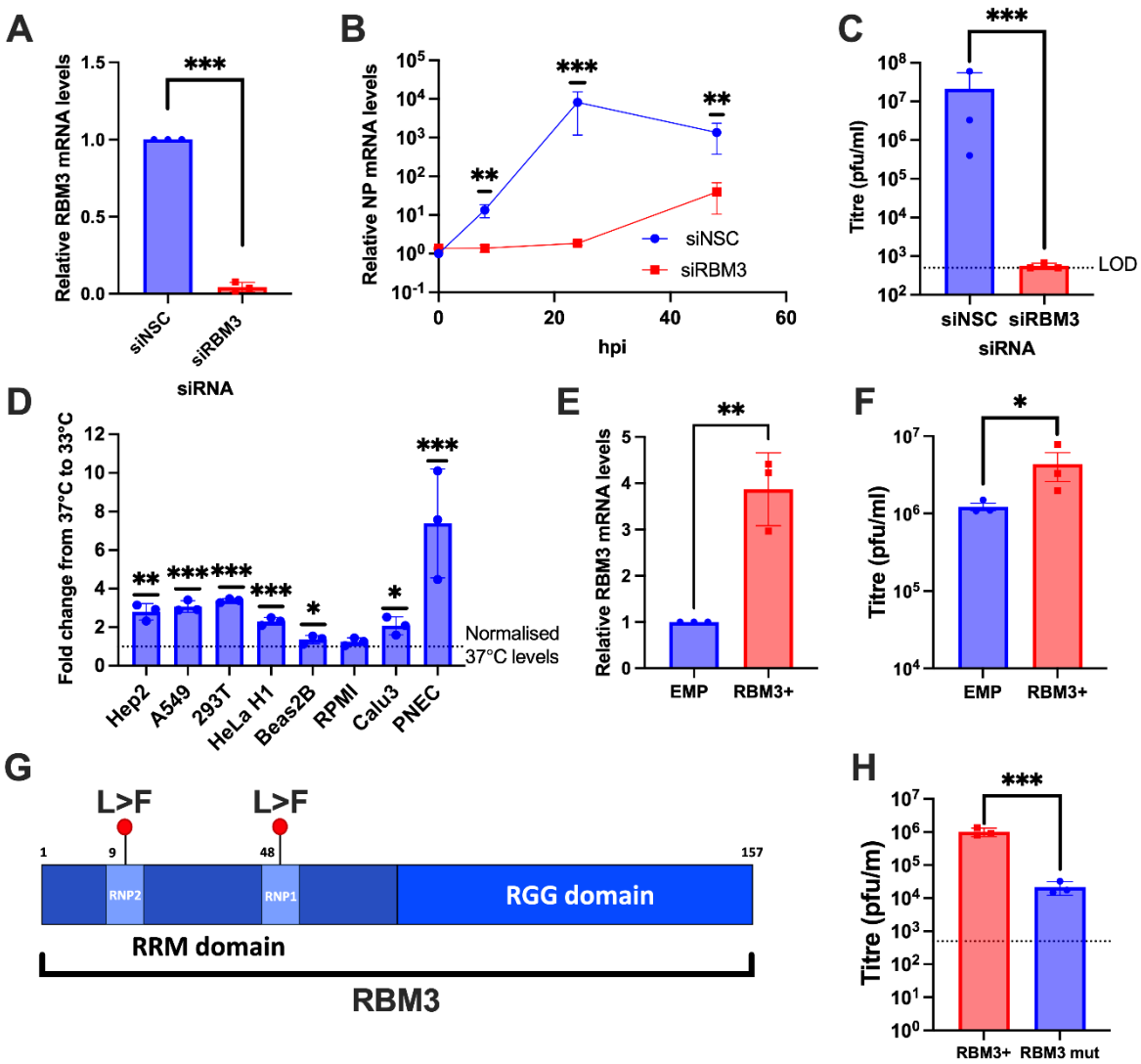

191

192 *Figure 2 – Reducing RBM3 levels in A549 cells greatly inhibits IAV replication.*

193 ***(A)*** *Quantification of RBM3 knockdown using RBM3-targeting siRNAs (siRBM3) compared to a nonspecific control siRNA*
194 *(siNSC).* ***(B)*** *Transcription levels of NP mRNA in siRBM3 or siNSC treated A549 cells infected with WSN at 37°C.* ***(C)*** *Viral titres*
195 *72 hpi with WSN MOI 0.01 in siRBM3 or siNSC treated cells.* ***(D)*** *Cold-responsiveness of a panel of cell lines and primary nasal*
196 *epithelial cells (PNECs) as determined by the induction of RBM3 expression by qPCR over 48 h and normalised to 37°C levels.*
197 ***(E)*** *Generation of a lentiviral RBM3 overexpression (RBM3+) A549 cell line alongside a control empty vector line (EMP).* ***(F)***
198 *Titres of WSN at 72 hpi after an MOI 0.01 infection in EMP or RBM3+ A549 cells.* ***(G)*** *Schematic representation of RBM3. Single*
199 *nonsense mutations were introduced into the RNA binding domains, RNP2 and RNP1, creating an RNA-binding null mutant*
200 *RBM3.* ***(H)*** *A549-RBM3+ or A549-RBM3 mut cells were infected at MOI 0.01 with WSN for 48 hours. Supernatants were*
201 *harvested and titrated. Dotted line indicates the limit of detection. Significance was determined using Student's t-test with*
202 **=p<0.05, **=p<0.01 and ***=p<0.001.*

203

204 With these cell lines in place, a direct interaction between RBM3 and viral transcripts could
205 next be established. To directly visualise the interaction between RBM3 and viral NP mRNA,
206 we employed proximity ligation assay coupled with fluorescence in situ hybridisation (PLA-
207 FISH) [28], a technique adapted here for the first time in the context of virus-infected cells
208 (Figure 3A). This approach revealed prominent cytoplasmic PLA signals in cells expressing
209 wild-type (WT) RBM3, indicating a specific and spatially distinct interaction with NP mRNA
210 (Figure 3B). In contrast, cells expressing either an empty vector or the RNA-binding-deficient
211 RBM3 mutant exhibited only low background signal, consistent with the loss of RNA-binding
212 capability. Notably, in WT RBM3-expressing cells, PLA spots were especially enriched at the
213 cytoplasmic face of the nuclear membrane. This localisation pattern may suggest that RBM3
214 engages NP mRNA soon after nuclear export, potentially stabilising viral transcripts at an early
215 post-transcriptional stage. These findings validate the specificity of RBM3–NP mRNA
216 interactions and highlight the utility of PLA-FISH in mapping host–viral RNA contacts with
217 subcellular resolution.

218 To further validate a direct interaction between RBM3 and NP mRNA we performed CLIP-
219 qPCR in A549-RBM3+ cells infected at MOI 3 for 6 h, then UV crosslinked, and subjected to
220 FLAG immunoprecipitation or an IgG control. The covalently bound RNA was then released by
221 proteinase K digestion, purified and analysed by qPCR. Flag-tagged RBM3 was efficiently
222 pulled down by an anti-Flag immunoprecipitation (Figure 3C & Supp Figure 3), with Actin used
223 as a control to show that this enrichment was specific. RBM3-bound RNA was evaluated by
224 qPCR to determine whether NP mRNA is strongly enriched in RBM3 pulldowns (Figure 3D),
225 due to the presence of multiple predicted high confidence motifs. We also quantified levels
226 of HA mRNA as a likely non-interactor and Actin mRNA, as a host mRNA. We observed a strong
227 and significant enrichment of NP mRNA between the RBM3-Flag and IgG control samples,

228 while no enrichment in HA or Actin levels was observed, indicating little or no binding with
229 RBM3. Taken together, these data collectively establish a direct interaction between RBM3
230 and NP viral mRNA transcripts, and that this predominantly takes place in the cytoplasm.
231 Finally, using RBPmap [29] and the published RBM3 binding motif (minimally GSNGSNG) [30],
232 we generated a prediction of the number of RBM3 high-confidence binding motifs on WSN
233 transcripts (Figure 3E). While every transcript contained at least 1 putative RBM3 motif with
234 $p<0.05$, NP mRNA was predicted to have multiple highly significant binding motifs with 3 sites
235 of $p<0.001$. Collectively, these data demonstrate that RBM3 directly interacts with NP mRNA
236 upon infection.

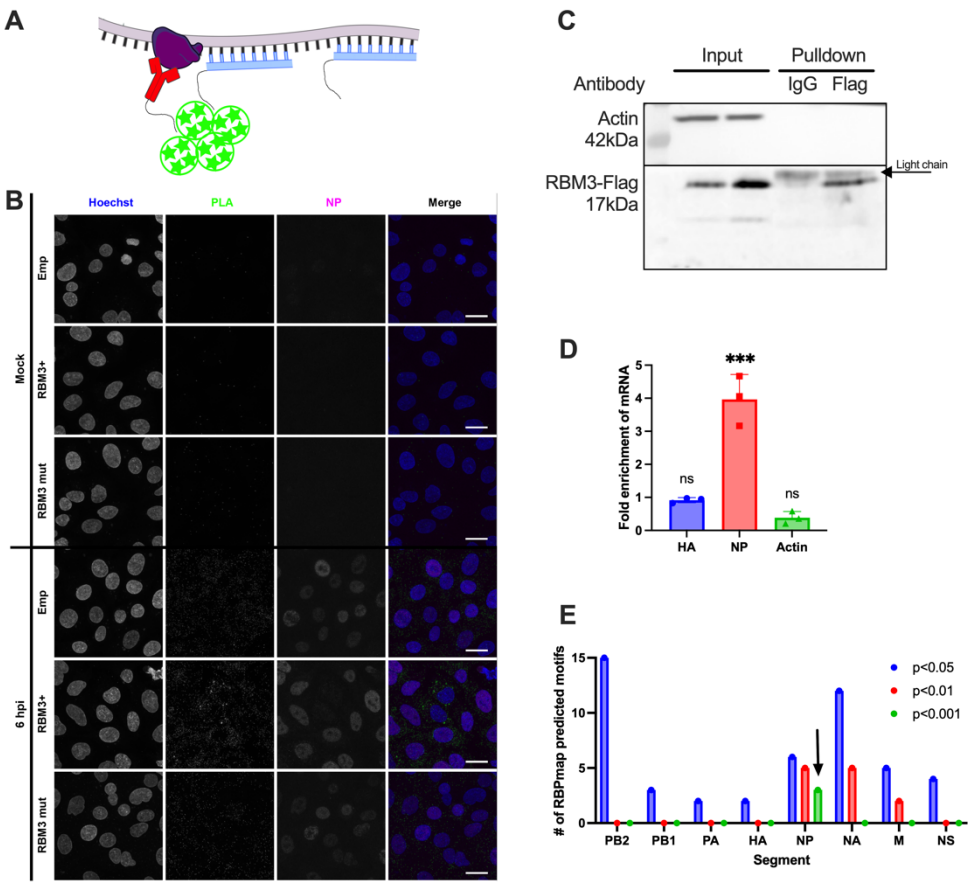

237

238 *Figure 3 – RBM3 directly associates with viral transcripts, increasing overall viral replication.*

239 ***(A)*** *Schematic of PLA-FISH, used to confirm a tight proximity between an RBP and a target mRNA, and the intracellular*
240 *localisation of this interaction.* ***(B)*** *Representative PLA-FISH images showing specific cytoplasmic NP mRNA–RBM3*
241 *interactions in WT RBM3-expressing cells, with prominent signal observed near the nuclear periphery, while only background*
242 *signal is detected in empty vector and RBM3 mutant controls. n=60 cells.* ***(C)*** *Western blot showing input and pulldown*

samples for CLIP-qPCR, blotting for Actin and overexpressed RBM3-Flag. ***(D)*** *qPCR quantification of the RNA extracted from CLIP samples demonstrated a significant increase in viral NP mRNA levels with minimal difference in HA or Actin transcript levels, when comparing RBM3 to IgG control pulldowns.* ***(E)*** *RBPmap predicted RBM3 binding motifs for each WSN positive strand segment, separated by predicted confidence of each motif.*

Overexpression of RBM3 and subsequent binding to NP mRNA stabilises transcripts

Having confirmed the interaction between RBM3 and NP mRNA, we next sought to identify how this interaction positively regulates WSN replication. Previous reports have suggested that RBM3 may stabilise certain bound transcripts in neuronal cells [21,22]. Given this context, we next explored the stability of a subset of viral transcripts in the A549-RBM3+ or empty vector A549 cells. Cells were infected with WSN at an MOI 3 for 6 h, then treated with actinomycin D to prevent further cellular and viral transcription [31]. Transcript levels were quantified hourly over 5 timepoints from 0-4 h post-actinomycin D treatment. The data were plotted to visualise the decay of RNA over this treatment period (Figure 4), with a one-phase decay model fitted to the data using a least squares regression. Observed differences in RNA stability were significantly different between cell lines and were assessed by comparing the decay constant (k) values using an extra sum-of-squares F test, with $p<0.05$ deemed significant. Although no significant effect on the stability of viral HA or M2 mRNA was observed (Figure 4A & B), a clear and significant increase in stability was quantified for NP mRNA with a >70% increase in RNA half-life (Figure 4C). Actinomycin D assays were then performed in A549-RBM3+ or the RBM3 RNA-binding mutant cell line after IAV infection. These revealed a loss of the stabilisation phenotype in the RBM3 mutant cells for viral NP transcripts as well as GAPDH (Figure 4D and Supp Figure 4). Interestingly, we also observed that overexpression of RBM3 significantly and positively regulated cellular GAPDH levels (Supp Figure 4A), with this phenotype again obviated in the RBM3mut cells. This suggests that RBM3 stabilisation is a direct result of RBM3 binding to target transcripts, and that this is likely a form of cellular post-transcriptional regulation for transcripts such as GAPDH, YAP1 [21] or

269 GAS6 [22]. This mechanism is then seemingly exploited by IAV during infection to promote
270 viral transcript stability upon nuclear export, and overall viral replication.

271 To be certain of our conclusions we employed a minimalist tethering approach. We set up a
272 reporter system in which 293T cells were transfected with a Renilla Luciferase encoding for
273 BoxB hairpins in the 3' UTR, and either WT RBM3 or LambdaN (λN)-RBM3 fusion protein
274 (Figure 4E). The 19 nt BoxB hairpin acts as the target sequence for λN binding and fusion of
275 λN with an RNA-binding protein allows for elucidation of the RBP's function on the BoxB-
276 encoded reporter RNA [32]. Actinomycin D assays were repeated 48 hours post-transfection
277 and levels of luciferase RNA were assessed by qPCR. A significant enhancement in transcript
278 half-life was observed upon expression of the fused λN-RBM3 protein (Figure 4F), providing
279 further evidence that supports the role of RBM3 as an mRNA stabilising agent.

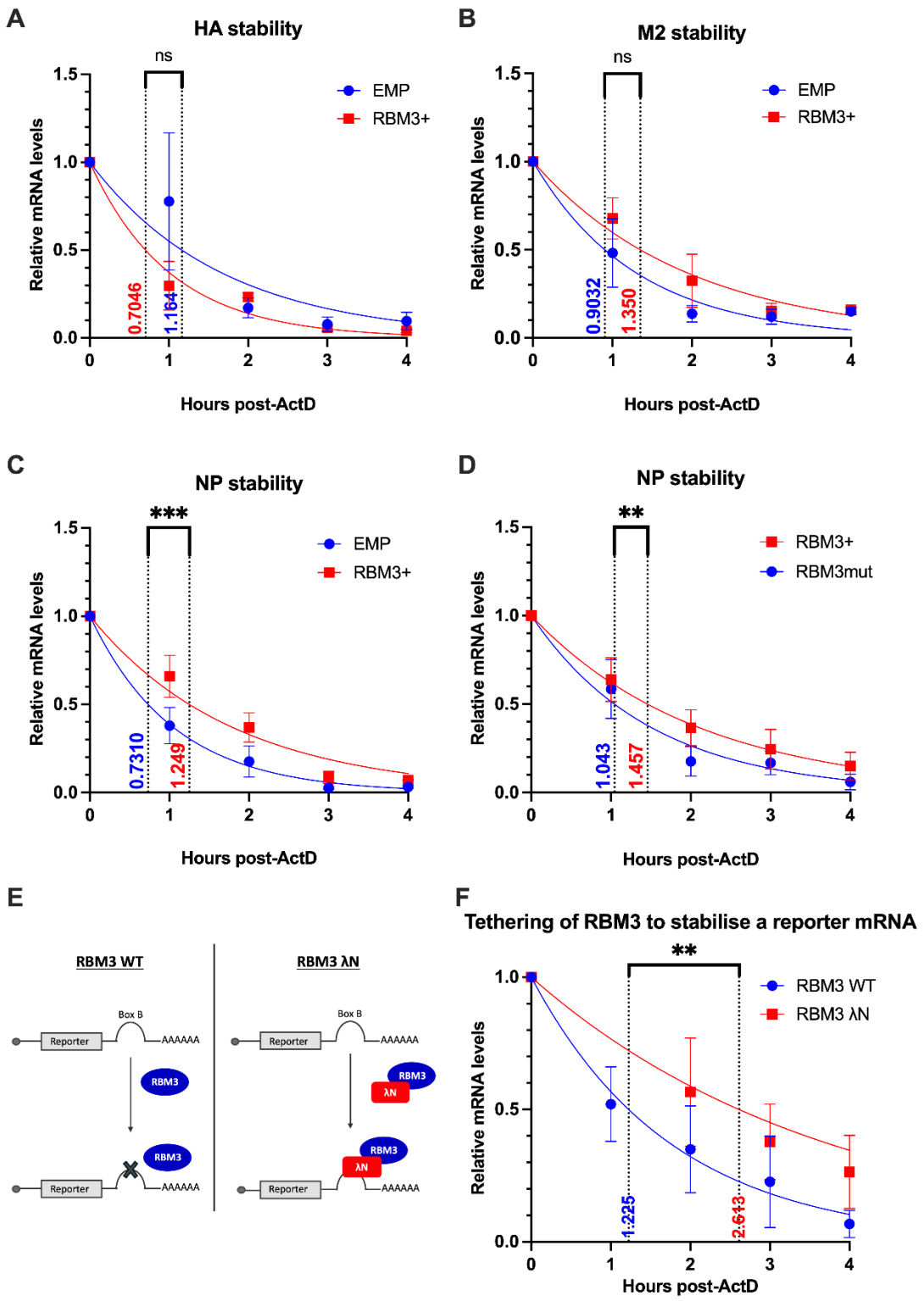

Figure 4 - RBM3 is a stabilising agent through directly binding to target mRNA including IAV NP mRNA.

*Transcript stability in empty vector (EMP) or RBM3 overexpression (RBM3+) A549 cells was established by an actinomycin D (ActD) assay commenced at 6 hpi. Viral transcripts HA **(A)**, M2 **(B)** and NP **(C)** were quantified over 5 hours with transcript half-life quantified by a one-phase decay using a least squares regression. **(D)** The same assay was performed in RBM3+ or the RBM3 RNA-binding mutant (RBM3mut) cell lines, with half-life quantified. **(E)** Schematic representation of the tethering reporter assay. **(F)** 293T cells were transfected with a Luciferase BoxB reporter alongside either WT RBM3 or fused λN-RBM3.*

287 *Cells were treated with Act D 48 hours post-transfection. Luciferase transcripts were quantified over 4 hours with transcript*
288 *half-lives quantified by a one-phase decay using a least squares regression.*

289 RBM3-NP mRNA complexes induce granule formation

290 IF analysis revealed striking cytoplasmic granule formation in WSN-infected cells
291 overexpressing wild-type RBM3 (WT). At both 6 and 8 hpi, RBM3 localised in multiple discrete
292 cytoplasmic foci (white arrows), which strongly colocalised with viral NP mRNA detected by
293 smiFISH, suggesting the assembly of RNA-protein granules involving both RBM3 and viral
294 transcripts (Figure 5). These granules were consistently observed across multiple fields but
295 noticeably increased in frequency between 6 and 8 hpi, implying that rising levels of NP mRNA
296 proliferated the formation of these granules (Figure 5).

297 In contrast, cells expressing the RNA-binding-deficient RBM3 mutant (MUT) or empty vector
298 (EMP) did not display granule formation at either time point. In these cells, RBM3 staining
299 was diffuse, and NP mRNA remained evenly distributed in the cytoplasm without foci (Figure
300 5). This absence of granules in MUT and EMP conditions highlights the requirement for
301 RBM3's RNA-binding capacity and sufficient protein expression for granule formation. The
302 consistent colocalisation of RBM3 and viral mRNA in the WT condition supports a model in
303 which, when expressed to sufficient levels, RBM3 drives the assembly of cytoplasmic RNA
304 granules during infection, potentially stabilising viral transcripts or modulating their
305 localisation.

306

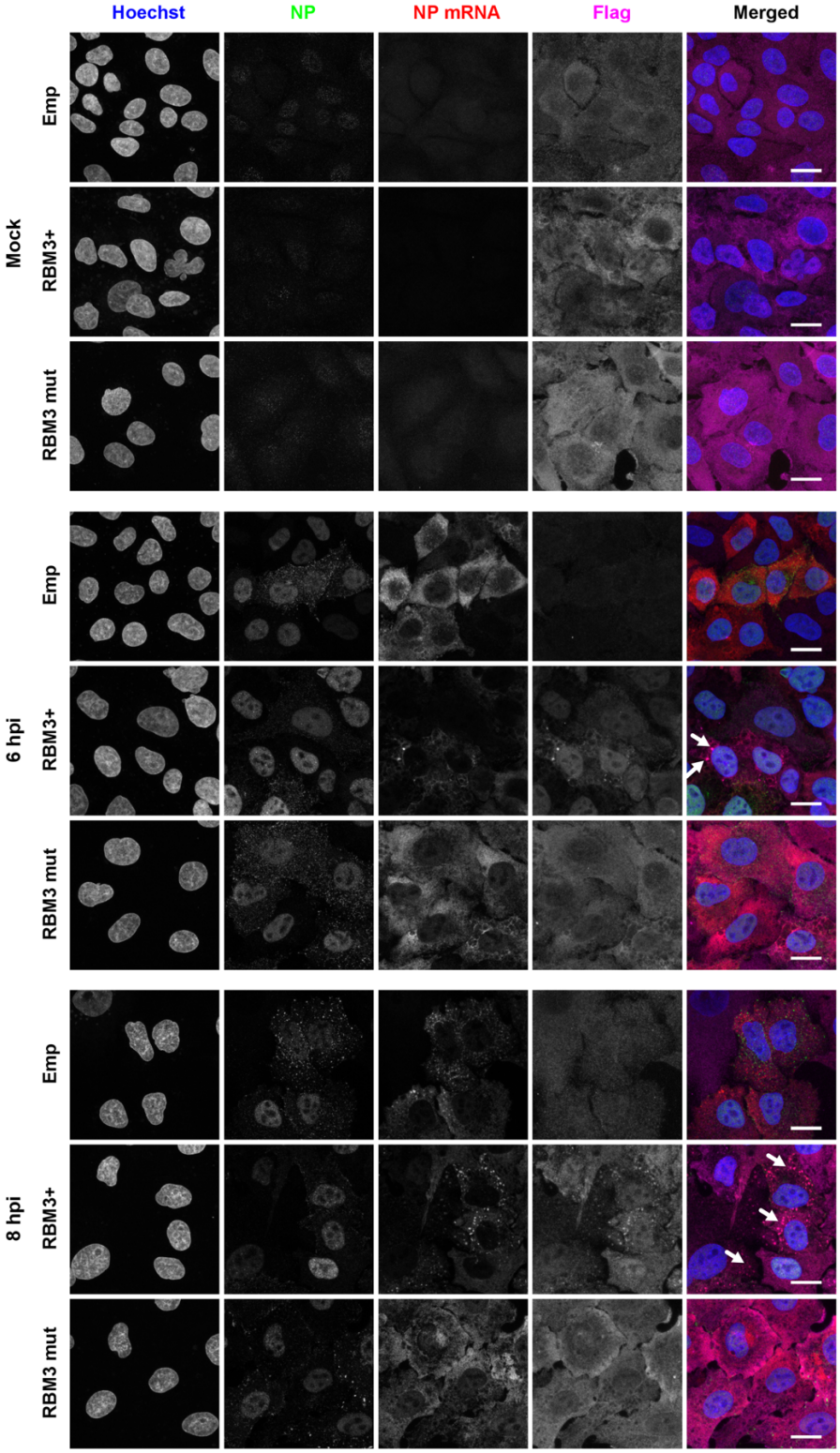

307

308 *Figure 5 – Formation of RBM3 and NP mRNA granules late in infection.*

309 *smiFISH of A/WSN/33 NP mRNA (Red) in Mock and infected A549-Emp, A549-RBM3+ and A549-RBM3 mut cells (MOI5, 6/8*
310 *hpi) was performed to determine the subcellular localisation of NP mRNA and to assess the colocalisation with RBM3+/mut.*
311 *Cells were stained to detect NP (green), Flag (Magenta) and Höchst (Blue). Scale Bar: 10 µM. Z stacks were acquired on Leica*
312 *STELLARIS ONE 660 tauSTED Nanoscope with a 100x objective with 1.4 NA. Images were analysed using Fiji/ImageJ version*
313 *1.54f.*

314

315 ASO-mediated increase of RBM3 levels in primary cells promotes overall viral replication

316 Finally, we wanted to determine whether RBM3-mediated increase of overall viral replication
317 would be mirrored in PNECs. Previous studies have determined that targeted ASO treatment
318 of the RBM3 poison exon Ex3a in immortalised cell lines can result in the exclusion of the
319 poison exon, preventing NMD of RBM3 transcripts, and thus increasing overall RBM3 levels,
320 effectively mimicking the function of HNRNPH1 [24]. Treatment of A549 cells with this
321 previously published Ex3a-specific ASO for 48 h resulted in an almost 4-fold increase in RBM3
322 transcript levels compared to that of a non-targeting control (Figure 6A), confirming its
323 effectiveness. Next, ASO treatment was applied apically to PNEC cultures from 3 donors.
324 Primary cells are much less permissive to transfection, therefore, ASO treatment would be
325 predicted to be much less effective at inducing RBM3 in these cultures. Nevertheless, we
326 observed a robust and significant ~50% increase in RBM3 transcript levels after 48 h
327 compared to the control ASO for all 3 donors (Figure 6B). Following this, we subjected PNEC
328 cultures from the same 3 donors to ASO treatment followed by infection with WSN for 48 h.
329 We then evaluated viral replication in these PNECS by quantification of viral RNA levels at 48
330 hpi. A significant increase in both NP mRNA and vRNA levels was observed by qPCR for each
331 donor upon treatment with the Ex3A-specific ASO, with mRNA levels on average more than
332 doubling after Ex3a ASO treatment (Figure 6C). These data confirm our earlier observations
333 that increasing RBM3 levels positively regulates IAV replication, in a highly relevant human
334 respiratory epithelial model of infection.

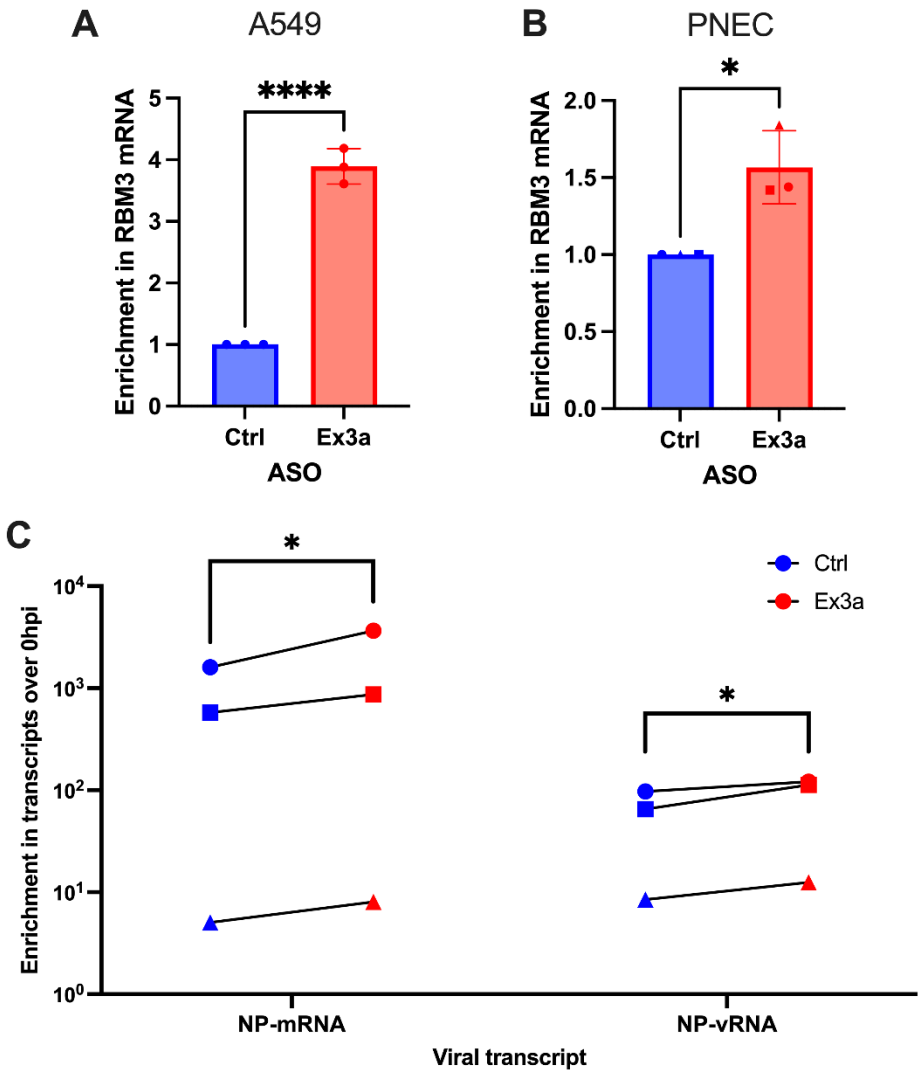

335

336 *Figure 6 - Increasing expression of RBM3 in PNECs significantly increases IAV replication*

337 ***(A)*** *Control (Ctrl) or Exon3a (Ex3a) specific ASOs were initially tested in A549 cells to determine their effectiveness in increasing*
338 *overall RBM3 mRNA levels, with an approximate 4-fold increase observed at 48 h post-transfection.* ***(B)*** *This was replicated*
339 *in PNECs at 48 h post-transfection where an approximate 50% ASO-mediated increase in RBM3 levels was quantified.* ***(C)***
340 *Quantifying viral mRNA and vRNA production in 3 donors (indicated by different shaped data points) previously treated with*
341 *Ctrl or Ex3a ASOs, demonstrated a significant increase in overall viral replication at 48 hpi.*

342

343 ## Discussion

344 Given the continuing risk of respiratory virus pandemics, due to coronaviruses such as SARS-
345 CoV-2 or zoonotic influenza strains like H5N1, a detailed understanding of virus-host
346 interactions in relevant tissue environments is critical for future preparedness. The upper
347 respiratory tract (URT) is a primary site of viral replication and transmission, particularly the
348 nasopharyngeal epithelium, which functions at cooler temperatures than core body
349 temperature (~33°C vs. 37°C). This cooler environment likely alters host cell biology and, in
350 turn, viral replication dynamics. To reduce transmission, it is essential to understand how
351 viruses exploit host factors in this unique tissue niche.

352 Here, we present a comprehensive, temperature-resolved RBPome, identifying RNA-binding
353 proteins (RBPs) that are differentially associated with mRNAs in A549 cells cultured at 33°C
354 compared to 37°C (Figure 1). This is the first high-resolution characterisation of the cold-
355 adapted RBPome in a context relevant to URT infection. We identified 63 RBPs unique to 33°C
356 and 151 unique to 37°C, with 209 shared across both conditions. Among these, the cold-
357 inducible protein RBM3 was significantly enriched at 33°C, suggesting temperature-
358 dependent regulation of host–RNA interactions.

359 RBM3, known to be regulated by HNRNPH1-mediated splicing [13], has been previously
360 implicated in cell survival under cold stress [33,34], and in stabilising mRNAs such as YAP1 and
361 GAS6 [21,22]. However, its role in viral RNA regulation remained largely unexplored. Our
362 study uncovers a previously underappreciated role for RBM3 as a direct stabiliser of IAV
363 mRNA, specifically the NP transcript. This discovery positions RBM3 as a critical modulator of
364 viral gene expression in the URT.

365 We employed multiple, orthogonal assays to robustly validate this interaction. RBM3
366 knockdown significantly reduced viral titres and NP mRNA levels (Figure 2B-C, Supp. Fig. 4),
367 while wild-type RBM3 overexpression enhanced replication. In contrast, an RNA-binding-
368 deficient mutant had no effect (Figure 2E-H), underlining the functional importance of RBM3's
369 RNA-binding capacity.

370 To directly assess RBM3–viral RNA interactions, we combined PLA-FISH (to detect close spatial
371 proximity in situ) and CLIP-qPCR (to confirm direct physical association), supported by in silico
372 binding motif prediction via RBPmap [29]. PLA-FISH revealed strong cytoplasmic co-
373 localisation between RBM3 and NP mRNA at 6 hpi, absent in the RNA-binding mutant (Figure
374 3B), while CLIP-qPCR confirmed direct enrichment of NP mRNA with RBM3 (Figure 3C-E).

375 Next, we explored the functional consequences of RBM3 binding on mRNA stability. RBM3
376 overexpression extended NP mRNA half-life (Figure 4C), an effect abolished in the RNA-
377 binding mutant (Figure 4D). We further validated this stabilising effect in a reporter-based
378 tethering assay, where recruitment of RBM3 to a 3' UTR significantly increased RNA stability
379 (Figure 4F). Together, these data demonstrate a clear and direct role for RBM3 in stabilising
380 viral transcripts, independent of indirect host responses.

381 In virus-infected cells, RBM3 overexpression also induced cytoplasmic granule formation that
382 co-localised with viral mRNAs (Figure 5), a phenotype absent in the mutant or under low
383 RBM3 expression. Given RBM3 is naturally upregulated at 33°C, our overexpression model
384 mimics URT-relevant conditions, suggesting that cooler temperatures promote protective
385 RNA granule formation that shields viral mRNAs from decay. This granule-based mechanism
386 likely contributes to elevated viral mRNA levels during infection.

387 To confirm the translational relevance of our findings, we tested whether increasing RBM3
388 levels in primary human nasal epithelial cells would alter IAV replication. Using ASO-mediated
389 induction of RBM3 [24], we observed donor-specific but consistently increased viral
390 replication, as reflected by elevated NP mRNA and vRNA levels (Figure 6). This demonstrates
391 the functional impact of RBM3 in a clinically relevant URT model.

392 Taken together, our data reveal that RBM3 plays a previously unrecognised, yet pivotal role
393 in stabilising IAV NP mRNA, enhancing replication particularly at cooler URT temperatures.
394 This stabilisation may occur via several mechanisms: protection from endonucleolytic
395 cleavage, inhibition of decay factor binding (e.g., exosome complex [35]), enhanced ribosome
396 loading [36], stabilisation of viral RNA structures [37], or modulation of epitranscriptomic
397 marks [38]. Alternatively, RBM3 may promote mRNA sequestration into membraneless
398 organelles already known to influence vRNA trafficking [39].

399 While IAV appears to have evolved to exploit RBM3 for replication efficiency in the URT, this
400 mechanism could be repurposed therapeutically. Given the success of mRNA vaccines for
401 SARS-CoV-2 [40], and ongoing development of nasal vaccine platforms to induce mucosal
402 immunity [41,42], RBM3's RNA-stabilising properties could be harnessed to enhance mRNA
403 stability and translation in future respiratory therapies. Notably, recent advances have shown
404 inhalable mRNA delivery to the airway epithelium in vivo [6], making this a viable direction
405 for translational research.

406 In conclusion, RBM3 is a temperature-sensitive host factor that directly binds and stabilises
407 influenza A virus mRNAs in the URT. Our multi-assay validation, the creation of a novel
408 temperature-specific RBPome, and the identification of a new functional axis in viral RNA
409 biology collectively underscore the originality and impact of this work. Beyond IAV, our
410 findings suggest that cold-inducible RBPs may represent a broader class of modulators

411 shaping respiratory virus replication in epithelial tissues. These insights expand our
412 understanding of host–pathogen interactions under physiologically relevant conditions and
413 open new avenues for therapeutic intervention and pandemic preparedness.
414

415 **Methods**

416 Cells

417 All immortalised cell lines were cultured in DMEM supplemented with 1% Pen-Strep (Thermo
418 Fisher Scientific; 15140122) and 5% FBS (Thermo Fisher Scientific; 10270106) at 37°C/33°C
419 and 5% CO_2. Cell lines used were A549s (ATCC; CCL-185), HEK 293Ts (ATCC; CRL-3216), MDCKs
420 (CCL-34), Hep2s (ATCC; CCL-23), HeLa H1s (ATCC; CRL-1958), Beas2Bs (ATCC; CRL-3588), RPMI
421 2650s (ATCC; CCL-30) and Calu3s (ATCC; HTB-55).

422 Virus stocks and infections

423 IAV WSN (A/WSN/33) stocks were generated from a reverse genetics system previously
424 described [43]. WSN stocks were grown on MDCK cells in IAV growth media consisting of
425 DMEM, Pen-Strep, 0.2% BSA (Merck; A8412), 25mM HEPES (Merck; H0887) and TPCK-trypsin
426 (Merck; T8802) and titrated on MDCK cells by plaque assay.

427 RIC

428 The protocol employed here to capture the RNA interactome of poly(A)+ RNA (RIC) from A549
429 cells has been described previously [18,25]. However, we made one minor modification. At
430 the time of seeding, 48 h before crosslinking and harvesting, A549 cells were either incubated
431 under the normal growth temperature of 37°C, to determine the 37°C RBPome, or incubated
432 in a 33°C incubator, to determine the 33°C RBPome. Cells were grown for 48 h at these
433 conditions before performing UV crosslinking at 254nm and lysis. The remaining steps were
434 followed exactly as has been described previously [25].

435 Protein visualisation

436 Western blotting was performed as has been previously described [44]. Primary antibodies
437 for influenza PA (Thermo Fisher Scientific; Pa5-32223), RBM3 (Proteintech; 14363-1-AP),
438 ACTB (Proteintech; 66009-1-ig), and Flag (Proteintech; 66008-3-ig) were all used at a 1:5000
439 dilution. Proteins bands on blots were visualised by chemiluminescence. Total protein was
440 imaged by silver staining (Thermo Fisher Scientific; 24612), following the manufacturer's
441 protocol.

442 LC-MS/MS and data analysis

443 Mass spectrometry of RIC samples was performed at the Cambridge Centre for Proteomics.
444 Sample treatment, preparation and trypsin digestion were performed as described previously
445 [45]. Data for each sample were acquired on an Orbitrap Fusion Lumos Tribrid mass
446 spectrometer over a 60 min run. No fractionation was performed due to the likely low
447 complexity of the sample. Raw mass spectrometry data was analysed using MaxQuant
448 software (v2.4.7.0) and utilising the Andromeda search engine [46]. The MS/MS spectra were
449 aligned to the Uniprot Homo sapiens protein database, with known mass spectrometry
450 contaminants and reversed sequences also included. The search was performed with trypsin
451 selected as the specific enzyme and a maximum of 2 missed cleavage events allowed. The MS
452 accuracy was set to 10 ppm, then 0.05 Da for the MS/MS. The maximum peptide charge was
453 set to seven and seven amino acids were required for the minimum peptide length. One
454 unique peptide to the protein group was required to call the presence of a specific protein,
455 while a false-discovery rate (FDR) of 1% was set. Statistical analysis to determine enriched
456 proteins in one set of biological samples over another was performed using the intensities
457 quantified by MaxQuant on Perseus software (v2.0.11) [47]. First, any potential contaminants,
458 reverse hits or proteins that were not well identified (fell below 1% FDR) were removed. Then

459 only proteins that were identified in at least 2 replicates from a single biological condition
460 were utilised. After filtering, the intensities were log transformed (log_2) and statistical
461 significance was calculated by way of an unpaired two-tailed Student's t-test for each protein
462 group. These values were then log transformed ($-log_{10}$) and the resulting p values and
463 enrichments were graphed as volcano plots. The cutoff for statistical significance was set to
464 $p < 0.05$.

465 siRNA knockdowns

466 A pair of siRNAs targeting the specified mRNA were used in each knockdown experiment,
467 aside from when a single non-specific control siRNA (siNSC) was used. Sequences of these
468 siRNAs are listed in Supplementary Table 3. A final concentration of 20nM total siRNA was
469 used, and these were transfected using Lipofectamine RNAiMAX (Invitrogen; 13778075)
470 following the manufacturer's instructions. A549 cells were seeded and transfected
471 simultaneously and incubated for 24 h, after which media was changed with fresh growth
472 media. Cells were then incubated for a further 24 h prior to infection.

473 IAV qPCR growth curves

474 A549 cells were infected with A/WSN/33 virus at an MOI 0.01 PFU/cell. At 0, 8, 24 and 48 hpi
475 RNA was extracted from cells using TRIzol (Invitrogen; 15596026). RNA was isolated and
476 precipitated following the manufacturer's instructions and 200ng was reverse transcribed
477 into cDNA using the ABI cDNA synthesis kit (Applied Biosystems; 4368814). For all cellular
478 targets RT was performed using an oligo dT, while viral RNA underwent separate RT reactions
479 with primers specific to each mRNA or vRNA [48]. These primers are listed in Supplementary
480 Table 4 alongside the primers used for qPCR amplification. All qPCR experiments were

481 performed using SYBR Select Master Mix (Applied Biosystems; 4472908) following the
482 manufacturer's instructions. All qPCR data were quantified using the ΔΔCT method.

483 Establishment of a RBM3 overexpression cell line using a lentiviral vector

484 A lentiviral expression plasmid was generated encoding for either a full length wild-type RBM3
485 C-terminally tagged with 2X Flag epitope tags (RBM3+), a full-length RNA-binding mutant
486 (RBM3-Mut), containing two single phenylalanine to leucine substitutions within RNP1 (L48F)
487 and RNP2 (L9F), or an empty vector (A549-EMP). A549-RBM3, A549-EMP and A549-Mut were
488 followed by a P2A self-cleaving peptide and a puromycin resistance gene, similar to a system
489 we have published previously [38]. Again, similar to previous publications, we rescued
490 lentiviral particles by co-transfecting 293T cells with the RBM3, RBM3 Mut or EMP lentiviral
491 vector alongside d8.74 (Addgene; 22036) and MD2G (Addgene; 12259). At 72 h post-
492 transfection the supernatant was harvested, passed through a 0.45 μm filter and then
493 overlaid onto fresh A549 cells. At 72 h post transduction cells were treated with 2 μg/ml
494 puromycin and left to select for 72 h. Cells were then single cell cloned in 96 well plates in the
495 presence of 2 μg/ml puromycin and left to grow for 3 weeks. Single cell colonies were then
496 selected, expanded, and checked by Western blot to confirm the expression of the transgene.

497 PLA-FISH

498 A549 cells expressing Flag, RBM3 WT or RBM3 Mt were seeded on to a 12 mm coverslip in 24
499 well plates. 24 hrs later cells were infected in a synchronised manner with IAV/WSN at an MOI
500 of 5 for 1 hr at 4°C. The infection was allowed to follow through for 6 hrs to allow for peak
501 viral mRNA production. 6 hrs later, cells were fixed with 4% PFA for 15 min at RT, then washed
502 thrice with PBS. Cells were permeabilised with 0.5% Triton X for 10 min at RT, then washed
503 thrice with PBS. Following a protocol adapted from Alagia et al. [28], coverslips were

504 incubated with 30 µl of PLA-blocking buffer in a pre-warmed humidified chamber and
505 incubated for 1 h at 37°C. Cells were incubated with 30 µl of FISH-PLA probe buffer in the
506 humidified chamber in a hybridisation oven at 95°C for 3 min, followed by 18 h incubation at
507 37°C. The next day, coverslips were placed into a 24 well plate and three washes were
508 performed with 2× SSC wash buffer, followed by two washes with PBS at 20°C for 5 min with
509 gentle rocking. Cells were incubated with 30 µl of Duolink Blocking Solution and incubated at
510 37°C for 1 h. Cells were incubated with 30 µl of primary antibody against Flag (Sigma, F1804)
511 diluted in Duolink Antibody Diluent for 18 h at 37°C in a humidified chamber. The next day,
512 coverslips were placed into a 24 well plate and three washes were performed with pre-
513 warmed Wash Buffer A at 20°C for 5 min with gentle rocking. Cells were incubated with 30 µl
514 of Minus PLA probe diluted 1:5 and Phalloidin diluted 1:200 in Duolink Antibody Diluent in a
515 humidity chamber at 37°C for 1 h followed by three washes with Wash Buffer A. Duolink ligase
516 buffer was diluted 1:5 in ddH2O. For 60 µL of ligase reaction solution, 1.5 µL of ligase enzyme
517 was added to 58.5 µL of the diluted Duolink ligase buffer dilution. Cells were incubated with
518 20 µl of ligase buffer in a humidity chamber at 37°C for 30 min followed by three washes with
519 Wash Buffer A. Duolink amplification buffer was diluted 1:5 in ddH2O and protected from
520 light. For a 60 µL of amplification reaction, 0.75 µL of polymerase enzyme was added to 59.25
521 µL of the diluted Duolink amplification buffer dilution. Cells were incubated with 20 µl of
522 amplification buffer in a humidity chamber at 37°C for 1h and 40 min followed by two washes
523 with pre-warmed Wash Buffer B containing 1:4000 Hoechst (Abcam; ab228551) in a 24 well
524 plate. Wash steps were performed at 20°C for 10 min with gentle rocking followed by a last
525 wash with 0.01× Wash Buffer B. Coverslips were mounted on to slides with Diamond antifade
526 Mounting medium and imaged the following day on the Leica STELLARIS ONE 660 tauSTED

527 Nanoscope with a 100x objective with 1.4 NA. Z stacks were acquired and analysed using
528 Fiji/ImageJ version 1.54f.

529 CLIP-qPCR

530 The CLIP-qPCR protocol employed here has been published previously [49]. Briefly, A549-
531 RBM3+ cells were seeded one day prior to infection. Cells were infected with A/WSN/33 at
532 an MOI 3 PFU/cell and incubated for 6 h. At 6 hpi media was removed from the cells, before
533 being washed in ice cold PBS. UV crosslinking was performed at 254nm. Cells were then
534 scraped, pelleted and lysed in 250 µl of NP40 lysis buffer (HEPES-KOH pH 7.5 50mM, KCl
535 150mM, EDTA pH 8.0 2mM, NaF 1mM and NP40 0.5%) on ice for 30 min. Lysates were clarified
536 by centrifugation and 10% of the sample was saved as an input and boiled in Laemmli buffer
537 containing 2% β-mercaptoethanol at 95°C for 10 min for western blotting. The remaining 90%
538 of lysate underwent immunoprecipitation with anti-Flag antibody (Merck, F1804) or IgG
539 control antibody coupled to Protein G Dynabeads (ThermoFisher, 10004D) for 1 h at room
540 temperature. Beads were then captured, washed five times with 1 mL NP40 lysis buffer and
541 three times with PBS. A fraction (10%) of the beads was removed, resuspended in Laemmli
542 buffer and boiled at 95°C for 10 min for Western blotting. The remaining 90% of beads
543 underwent proteinase K digestion (ThermoFisher, EO0491) at 55°C for 60 min to release
544 bound RNA, following the manufacturer's instructions. RNA was then isolated from the
545 digestion by TRIzol LS (ThermoFisher, 10296028) and ethanol precipitation and cDNA were
546 synthesized using oligo dT or A/WSN/33 specific primers [48] (Supplementary Table 4).
547 Quantification of the cDNAs was performed by qPCR, as described below. Fold enrichment of
548 RNA levels was quantified using the ΔΔCT method and normalised to input levels.

549 Actinomycin D assays

550 A549-RBM3+, A549-Mut and A549-EMP cells were seeded at a density of 1 x 10^5 cells/well
551 one day prior to infection. Cells were infected with WSN at a MOI of 3 PFU/cell. At 6 hpi, RNA
552 was harvested from a single well for each cell type, constituting the 0 h timepoint. All
553 remaining infected wells underwent media exchange for growth media containing 2 µg/mL
554 Actinomycin D (SBR00013). RNA was harvested hourly from 7-10 hpi representing 1-4 h post
555 Actinomycin D treatment. RNA underwent cDNA conversion using oligo dT or A/WSN/33
556 specific primers, with the ABI cDNA synthesis kit (Applied Biosystems; 4368814).
557 Quantification of the cDNAs was performed by qPCR, described above. Fold enrichment of
558 RNA levels was quantified using the ΔΔCT method and normalised to either A549-EMP or
559 A549-RBM3 levels.

560 <u>λN tethering assay</u>

561 λN was cloned into a lentiviral expression vector expressing full-length WT RBM3. 293T cells
562 were seeded at a density of 1 x 10^5 cells/mL in a 12-well plate the day before transfection.
563 The following day, cells were transfected with 500 ng of pCI-RLuc-BoxB [50] and 100 ng of
564 either the WT RBM3 or the λN-RBM3 WT expressing plasmids. At 48 hours post-transfection,
565 RNA was harvested from a single well for each transfection to represent a 0h timepoint. All
566 remaining cells were treated with 2 µg/mL Actinomycin D (SBR00013). RNA was harvested by
567 TRIzol hourly up to 4 hours post-treatment. RNA underwent DNaseI (Invitrogen, EN0521)
568 digestion to remove any residual plasmid DNA before cDNA conversion using oligo dT primers
569 with the ABI cDNA synthesis kit (Applied Biosystems; 4368814). Quantification of the cDNAs
570 was performed by qPCR, described above. Fold enrichment of luciferase RNA levels was
571 quantified using the ΔΔCT method and normalised to the corresponding 0 h mRNA levels.

572 <u>Immunofluorescence</u>

573 A549-Emp, A549-RBM3+, A549-RBM3 mut cells were seeded in 24-well plates onto 12 mm
574 coverslips. 24h post seeding, cells were infected with influenza A/WSN/33 at MOI 5. Cells
575 were fixed at 6 hpi with 4% PFA and permeabilised with 70% ethanol for 2 hours at 4°C. Cells
576 were briefly washed with FISH wash buffer (10% SSC, 10% formamide, 80% ddH2O) and
577 incubated O/N at 37°C with smiFISH probes (Supplementary Table 6) against WSN NP mRNA
578 annealed to a Cy3 imager strand, as we have previously described [17]. Cells were washed
579 twice with FISH wash buffer at 37°C for 30 minutes. Cells were stained with primary antibodies
580 Rabbit anti-NP (PA5-32242, Invitrogen) and Mouse anti-Flag (66008-3-ig, Proteintech) to
581 detect RBM3+/mut for 1 hr at 37°C, followed by Goat anti-Ms AF647 (A32728, Invitrogen) and
582 Goat anti-Rb AF488 (A11008, Invitrogen) secondary antibodies. Cells were counterstained
583 with Hoechst (ab228551, abcam) and mounted using ProLong™ Diamond antifade mounting
584 media (P36961, Invitrogen). Coverslips were imaged with a Leica STELLARIS ONE 660 tauSTED
585 Nanoscope with a 100x objective with 1.4 NA. Z stacks were acquired and analysed using
586 Fiji/ImageJ version 1.54f.

587 Well-Differentiated Primary Airway Epithelial Cell Culture

588 Primary nasal epithelial cells were obtained from Promocell and well differentiated primary
589 nasal epithelial cell (WD-PNEC) cultures were established as described previously [51]. Briefly,
590 WD-PNECs were seeded onto collagen coated 6 mm Transwells (Sarstedt, 83.3932.041) at
591 $3x10^4$ cells/transwell. Cells were submerged in modified Promocell Airway Epithelial Cell
592 Growth Medium which was replaced on the apical and basal side every 2 days until the cells
593 reached confluency. Once confluent, an air liquid interface (ALI) was initiated by completely
594 removing the apical medium. Cells were differentiated using Pneumacult ALI medium
595 (Stemcell Technologies, #05001) supplemented with hydrocortisone and heparin. For

596 downstream experiments, WD-PNECs were only used when there was extensive cilia
597 coverage and mucus production, clear hallmarks of full differentiation.

598 ASO transfection and IAV infection of cells

599 A549s were transfected with control or Exon 3a targeting ASOs [24] (Supplementary Table 5)
600 to initially test whether induction of RBM3 could be achieved in airway cells. ASOs were
601 resuspended in DMEM at a concentration of 1 µM and transfected using Lipofectamine 2000
602 (Invitrogen, 1 µL/mL). At 48 h post-transfection RNA was harvested, cDNA synthesised as
603 described above, and RBM3 levels quantified by qPCR. For WD-PNEC cells, the transfection
604 conditions were the same, with the ASO-containing transfection mix added apically to WD-
605 PNECs. Cells were incubated for 48 h prior to infection with WSN MOI 0.01 PFU/cell in DMEM.
606 At 1 hpi, the inoculum was removed and transwells were washed 5 times in DMEM to remove
607 unbound virus. RNA was harvested from WD-PNECS using Trizol™ either before infection or
608 at 72 hours post-infection.

609 Statistical analysis

610 Unless otherwise stated, all experiments were performed as 3 independent biological
611 replicates. When bar graphs are used to represent the data, each individual replicate can be
612 observed as a point overlaid on the bar, with error bars indicating standard deviation.
613 Significance was calculated by performing Student's t-test with * indicating $p<0.05$, **
614 indicating $p<0.01$ and *** indicating $p<0.001$.

615

616 **Acknowledgements**

617 This research was funded in part by an ERC-STG grant, PTFLU 949506 awarded to D.G.C. This
618 research received infrastructure support from the Wellcome-Wolfson Institute for
619 Experimental Medicine at Queen's University Belfast. Authors would like to thank Dr Seyed
620 Mehdi Jafarnejad for providing the plasmids for the BoxB reporter system.

621 In Figure 1 cells_bilayer icon by Marcel Tisch is licensed under CC0, upper-respiratory-tract
622 icon by Servier https://smart.servier.com/ is licensed under CC-BY 3.0 Unported, lung icon by
623 Servier https://smart.servier.com/ is licensed under CC-BY 3.0 Unported, all protein icons by
624 Servier https://smart.servier.com/ is licensed under CC-BY 3.0 Unported,
625 Liquid_Chromatograph_Mass_Spectrometer icon by DBCLS
626 https://togotv.dbcls.jp/en/pics.html is licensed under CC-BY 4.0 Unported and rna icon by
627 Servier https://smart.servier.com/ is licensed under CC-BY 3.0 Unported. In Figure 3 RNA,
628 oligo, RBP and antibody icons were acquired from the NIAID NIH BIOART under a CC-BY
629 license.

630

631 **References**

632 1. Lakdawala SS, Jayaraman A, Halpin RA, Lamirande EW, Shih AR, Stockwell TB, et
633 al. The soft palate is an important site of adaptation for transmissible influenza
634 viruses. Nature. 2015;526: 122–125. doi:10.1038/nature15379

635 2. Xie C, Su W, Sia SF, Choy KT, Morrell S, Zhou J, et al. A(H1N1)pdm09 Influenza
636 Viruses Replicating in Ferret Upper or Lower Respiratory Tract Differed in
637 Onward Transmission Potential by Air. J Infect Dis. 2022;225: 65–74.
638 doi:10.1093/INFDIS/JIAB286

639 3. Richard M, van den Brand JMA, Bestebroer TM, Lexmond P, de Meulder D,
640 Fouchier RAM, et al. Influenza A viruses are transmitted via the air from the nasal
641 respiratory epithelium of ferrets. Nature Communications 2020 11:1. 2020;11:
642 1–11. doi:10.1038/s41467-020-14626-0

643 4. Varble A, Albrecht RA, Backes S, Crumiller M, Bouvier NM, Sachs D, et al.
644 Influenza A Virus Transmission Bottlenecks Are Defined by Infection Route and
645 Recipient Host. Cell Host Microbe. 2014;16: 691–700.
646 doi:10.1016/J.CHOM.2014.09.020

647 5. Bisht K, te Velthuis AJW. Decoding the Role of Temperature in RNA Virus
648 Infections. mBio. 2022;13. doi:10.1128/MBIO.02021-22/ASSET/C4C1EBDE-
649 A0D5-410C-9B3C-4C65FBA3C93F/ASSETS/IMAGES/MEDIUM/MBIO.02021-22-
650 F002.GIF

651 6. Suberi A, Grun MK, Mao T, Israelow B, Reschke M, Grundler J, et al. Polymer
652 nanoparticles deliver mRNA to the lung for mucosal vaccination. Sci Transl Med.
653 2023;15.

654 doi:10.1126/SCITRANSLMED.ABQ0603/SUPPL_FILE/SCITRANSLMED.ABQ0603_
655 MDAR_REPRODUCIBILITY_CHECKLIST.PDF
656 7. McMahan K, Wegmann F, Aid M, Sciacca M, Liu J, Hachmann NP, et al. Mucosal
657 boosting enhances vaccine protection against SARS-CoV-2 in macaques. Nature
658 2023 626:7998. 2023;626: 385–391. doi:10.1038/s41586-023-06951-3
659 8. Eccles R. Why is temperature sensitivity important for the success of common
660 respiratory viruses? Rev Med Virol. 2021;31: 1–8. doi:10.1002/RMV.2153
661 9. Otter CJ, Fausto A, Tan LH, Khosla AS, Cohen NA, Weiss SR. Infection of primary
662 nasal epithelial cells differentiates among lethal and seasonal human
663 coronaviruses. Proc Natl Acad Sci U S A. 2023;120: e2218083120.
664 doi:10.1073/PNAS.2218083120/SUPPL_FILE/PNAS.2218083120.SAPP.PDF
665 10. Pullara P, Alshareedah I, Banerjee PR. Temperature-dependent reentrant phase
666 transition of RNA-polycation mixtures. Soft Matter. 2022;18: 1342–1349.
667 doi:10.1039/D1SM01557E
668 11. Riback JA, Katanski CD, Kear-Scott JL, Pilipenko E V., Rojek AE, Sosnick TR, et al.
669 Stress-Triggered Phase Separation Is an Adaptive, Evolutionarily Tuned
670 Response. Cell. 2017;168: 1028-1040.e19. doi:10.1016/J.CELL.2017.02.027
671 12. Tauber D, Tauber G, Parker R. Mechanisms and Regulation of RNA Condensation
672 in RNP Granule Formation. Trends Biochem Sci. 2020;45: 764–778.
673 doi:10.1016/J.TIBS.2020.05.002
674 13. Lin JQ, Khuperkar D, Pavlou S, Makarchuk S, Patikas N, Lee FC, et al. HNRNPH1
675 regulates the neuroprotective cold-shock protein RBM3 expression through

676 poison exon exclusion. EMBO J. 2023;42: e113168.
677 doi:10.15252/EMBJ.2022113168

678 14. Bonazza S, Courtney DG. Influenza A virus RNA localisation and the interceding
679 trafficking pathways of the host cell. PLoS Pathog. 2025;21: e1013090.
680 doi:10.1371/JOURNAL.PPAT.1013090

681 15. Cugusi S, Mitter R, Kelly GP, Walker J, Han Z, Pisano P, et al. Heat shock induces
682 premature transcript termination and reconfigures the human transcriptome.
683 Mol Cell. 2022;82: 1573-1588.e10.
684 doi:10.1016/J.MOLCEL.2022.01.007/ATTACHMENT/F4235ADB-517D-41B2-
685 B14B-196321576620/MMC5

686 16. Gagnon D, Barry H, Barhdadi A, Oussaid E, Mongrain I, Lemieux Perreault LP, et
687 al. A dataset of proteomic changes during human heat stress and heat
688 acclimation. Scientific Data 2023 10:1. 2023;10: 1–6. doi:10.1038/s41597-023-
689 02809-5

690 17. Bonazza S, Coutts HL, Sukumar S, Turkington HL, Courtney DG. Identifying
691 cellular RNA-binding proteins during infection uncovers a role for MKRN2 in
692 influenza mRNA trafficking. Schwemmle M, editor. PLoS Pathog. 2024;20:
693 e1012231. doi:10.1371/journal.ppat.1012231

694 18. Garcia-Moreno M, Noerenberg M, Ni S, Järvelin AI, González-Almela E, Lenz CE,
695 et al. System-wide Profiling of RNA-Binding Proteins Uncovers Key Regulators of
696 Virus Infection. Mol Cell. 2019;74: 196-211.e11.
697 doi:10.1016/j.molcel.2019.01.017

698 19. Schmidt N, Ganskih S, Wei Y, Gabel A, Zielinski S, Keshishian H, et al. SND1 binds
699 SARS-CoV-2 negative-sense RNA and promotes viral RNA synthesis through
700 NSP9. Cell. 2023;186: 4834-4850.e23. doi:10.1016/J.CELL.2023.09.002

701 20. Kamel W, Noerenberg M, Cerikan B, Chen H, Järvelin AI, Kammoun M, et al.
702 Global analysis of protein-RNA interactions in SARS-CoV-2 infected cells reveals
703 key regulators of infection. Mol Cell. 2021 [cited 25 May 2021].
704 doi:10.1016/j.molcel.2021.05.023

705 21. Xia W, Su L, Jiao J. Cold-induced protein RBM3 orchestrates neurogenesis via
706 modulating Yap mRNA stability in cold stress. J Cell Biol. 2018;217: 3464–3479.
707 doi:10.1083/JCB.201801143

708 22. Lin P, Lin C, Diao L. RBM3 Ameliorates Acute Brain Injury-induced Inflammation
709 and Oxidative Stress by Stabilizing GAS6 mRNA Through Nrf2 Signaling Pathway.
710 Neuroscience. 2024;547: 74–87. doi:10.1016/J.NEUROSCIENCE.2024.03.028

711 23. Dupont M, Krischuns T, Gianetto QG, Paisant S, Bonazza S, Brault J-B, et al. The
712 RBPome of influenza A virus NP-mRNA reveals a role for TDP-43 in viral
713 replication. Nucleic Acids Res. 2024;52. doi:10.1093/NAR/GKAE291

714 24. Preußner M, Smith HL, Hughes D, Zhang M, Emmerichs A, Scalzitti S, et al. ASO
715 targeting RBM3 temperature-controlled poison exon splicing prevents
716 neurodegeneration in vivo . EMBO Mol Med. 2023;15. Available:
717 https://www.embopress.org/doi/10.15252/emmm.202217157

718 25. Castello A, Fischer B, Eichelbaum K, Horos R, Beckmann BM, Strein C, et al.
719 Insights into RNA Biology from an Atlas of Mammalian mRNA-Binding Proteins.
720 Cell. 2012;149: 1393–1406. doi:10.1016/j.cell.2012.04.031

721 26. RB Z, XL L, CY Z, DC Y. RNA binding motif protein 3: a potential biomarker in
722 cancer and therapeutic target in neuroprotection. Oncotarget. 2017;8.
723 doi:10.18632/ONCOTARGET.14755
724 27. Serin G, Joseph G, Ghisolfi L, Bauzan M, Erard M, Amalric F, et al. Two RNA-
725 binding domains determine the RNA-binding specificity of nucleolin. J Biol Chem.
726 1997;272: 13109–13116. doi:10.1074/JBC.272.20.13109
727 28. Alagia A, Ketley RF, Gullerova M. Detecting RNA-protein proximity at DNA
728 double-strand breaks using combined fluorescence in situ hybridization with
729 proximity ligation assay. STAR Protoc. 2023;4. doi:10.1016/J.XPRO.2023.102096
730 29. Paz I, Kosti I, Ares M, Cline M, Mandel-Gutfreund Y. RBPmap: a web server for
731 mapping binding sites of RNA-binding proteins. Nucleic Acids Res. 2014;42.
732 doi:10.1093/NAR/GKU406
733 30. Liu Y, Hu W, Murakawa Y, Yin J, Wang G, Landthaler M, et al. Cold-induced RNA-
734 binding proteins regulate circadian gene expression by controlling alternative
735 polyadenylation. Scientific Reports 2013 3:1. 2013;3: 1–11.
736 doi:10.1038/srep02054
737 31. Ratnadiwakara M, Änkö M-L. mRNA Stability Assay Using transcription inhibition
738 by Actinomycin D in Mouse Pluripotent Stem Cells. Bio Protoc. 2018;8.
739 doi:10.21769/BIOPROTOC.3072
740 32. Baron-Benhamou J, Gehring NH, Kulozik AE, Hentze MW. Using the λN peptide
741 to tether proteins to RNAs. mRNA Processing and Metabolism Methods in
742 Molecular Biology . Humana Press; 2004.

743 33. Peretti D, Bastide A, Radford H, Verity N, Molloy C, Martin MG, et al. RBM3
744 mediates structural plasticity and protective effects of cooling in
745 neurodegeneration. Nature. 2015;518: 236–239. doi:10.1038/NATURE14142

746 34. Wellmann S, Truss M, Bruder E, Tornillo L, Zelmer A, Seeger K, et al. The RNA-
747 Binding Protein RBM3 Is Required for Cell Proliferation and Protects Against
748 Serum Deprivation-Induced Cell Death. Pediatric Research 2010 67:1. 2010;67:
749 35–41. doi:10.1203/pdr.0b013e3181c13326

750 35. Schmid M, Jensen TH. The exosome: a multipurpose RNA-decay machine. Trends
751 Biochem Sci. 2008;33: 501–510. doi:10.1016/j.tibs.2008.07.003

752 36. Dresios J, Aschrafi A, Owens GC, Vanderklish PW, Edelman GM, Mauro VP. Cold
753 stress-induced protein Rbm3 binds 60S ribosomal subunits, alter microRNA
754 levels, and enhances global protein synthesis. Proc Natl Acad Sci U S A. 2005;102:
755 1865–1870. doi:10.1073/PNAS.0409764102/SUPPL_FILE/09764FIG7.JPG

756 37. Yang R, Pan M, Guo J, Huang Y, Zhang QC, Deng T, et al. Mapping of the influenza
757 A virus genome RNA structure and interactions reveals essential elements of
758 viral replication. Cell Rep. 2024;43. doi:10.1016/J.CELREP.2024.113833

759 38. Courtney DG, Kennedy EM, Dumm RE, Bogerd HP, Tsai K, Heaton NS, et al.
760 Epitranscriptomic Enhancement of Influenza A Virus Gene Expression and
761 Replication. Cell Host Microbe. 2017;22: 377–386.
762 doi:10.1016/j.chom.2017.08.004

763 39. Alenquer M, Vale-Costa S, Etibor TA, Ferreira F, Sousa AL, Amorim MJ. Influenza
764 A virus ribonucleoproteins form liquid organelles at endoplasmic reticulum exit
765 sites. Nat Commun. 2019;10. doi:10.1038/S41467-019-09549-4

766 40. Morens DM, Taubenberger JK, Fauci AS. Rethinking next-generation vaccines for
767 coronaviruses, influenzaviruses, and other respiratory viruses. Cell Host
768 Microbe. 2023;31: 146–157. doi:10.1016/J.CHOM.2022.11.016

769 41. Sheikh-Mohamed S, Isho B, Chao GYC, Zuo M, Cohen C, Lustig Y, et al. Systemic
770 and mucosal IgA responses are variably induced in response to SARS-CoV-2
771 mRNA vaccination and are associated with protection against subsequent
772 infection. Mucosal Immunol. 2022;15: 799. doi:10.1038/S41385-022-00511-0

773 42. Liew F, Talwar S, Cross A, Willett BJ, Scott S, Logan N, et al. SARS-CoV-2-specific
774 nasal IgA wanes 9 months after hospitalisation with COVID-19 and is not induced
775 by subsequent vaccination. EBioMedicine. 2023;87: 104402.
776 doi:10.1016/J.EBIOM.2022.104402

777 43. Fodor E, Devenish L, Engelhardt OG, Palese P, Brownlee GG, García-Sastre A.
778 Rescue of Influenza A Virus from Recombinant DNA. J Virol. 1999;73: 9679.
779 doi:10.1128/JVI.73.11.9679-9682.1999

780 44. Courtney DG, Chalem A, Bogerd HP, Law BA, Kennedy EM, Holley CL, et al.
781 Extensive epitranscriptomic methylation of A and C residues on murine leukemia
782 virus transcripts enhances viral gene expression. mBio. 2019;10: e01209-19.
783 doi:http://dx.doi.org/10.1101/591545

784 45. Queiroz RML, Smith T, Villanueva E, Marti-Solano M, Monti M, Pizzinga M, et al.
785 Comprehensive identification of RNA–protein interactions in any organism using
786 orthogonal organic phase separation (OOPS). Nature Biotechnology 2019 37:2.
787 2019;37: 169–178. doi:10.1038/s41587-018-0001-2

788 46. Cox J, Mann M. MaxQuant enables high peptide identification rates,
789 individualized p.p.b.-range mass accuracies and proteome-wide protein
790 quantification. Nature Biotechnology 2008 26:12. 2008;26: 1367–1372.
791 doi:10.1038/nbt.1511

792 47. Tyanova S, Temu T, Sinitcyn P, Carlson A, Hein MY, Geiger T, et al. The Perseus
793 computational platform for comprehensive analysis of (prote)omics data.
794 Nature Methods 2016 13:9. 2016;13: 731–740. doi:10.1038/nmeth.3901

795 48. Kawakami E, Watanabe T, Fujii K, Goto H, Watanabe S, Noda T, et al. Strand-
796 specific real-time RT-PCR for distinguishing influenza vRNA, cRNA, and mRNA. J
797 Virol Methods. 2011;173: 1. doi:10.1016/J.JVIROMET.2010.12.014

798 49. Courtney DG, Tsai K, Bogerd HP, Kennedy EM, Law BA, Emery A, et al.
799 Epitranscriptomic Addition of m5C to HIV-1 Transcripts Regulates Viral Gene
800 Expression. Cell Host Microbe. 2019;26: 217–227.
801 doi:10.1016/j.chom.2019.07.005

802 50. Choi JH, Luo J, Hesketh GG, Guo S, Pistofidis A, Ladak RJ, et al. Repression of
803 mRNA translation initiation by GIGYF1 via disrupting the eIF3-eIF4G1
804 interaction. Sci Adv. 2024;10: eadl5638. doi:10.1126/SCIADV.ADL5638

805 51. Broadbent L, Villenave R, Guo-Parke H, Douglas I, Shields MD, Power UF. In Vitro
806 Modeling of RSV Infection and Cytopathogenesis in Well-Differentiated Human
807 Primary Airway Epithelial Cells (WD-PAECs). Methods Mol Biol. 2016;1442: 119–
808 139. doi:10.1007/978-1-4939-3687-8_9

809

810

811 **Supplementary data**

812 Supplementary Table 1 – Initial RIC dataset prior to downstream analysis

813 Supplementary Table 2 – RIC dataset of RBP identified in at least 2 replicates of each

814 condition, with fold enrichment and p values included.

815 Supplementary Table 3 – siRNA sequences

816 Supplementary Table 4 – Primer sequences

817 Supplementary Table 5 – Sequences of antisense oligonucleotides

818 Supplementary Table 6 – smiFISH probe sequences

819

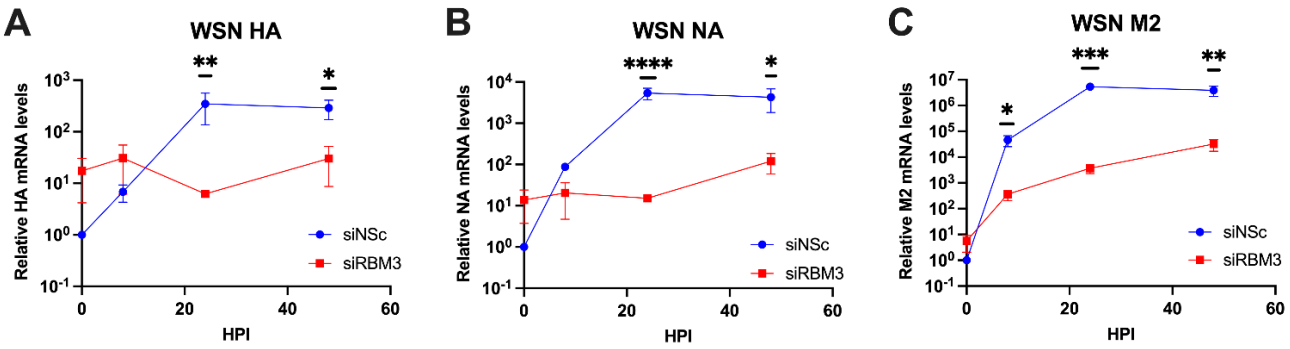

820

821 *Supplementary Figure 1 – IAV transcript levels upon loss of RBM3.*

822 *A549 cells were initially transfected with a negative control NSC siRNA or an RBM3-targeting siRNA and incubated for 48h.*
823 *RNA was harvested from these cells after infection with WSN at an MOI 0.01 and further incubation for 0, 8, 24 or 48 hpi.*
824 *Individual viral transcript levels were quantified by qPCR and normalised to GAPDH levels. Upon loss of RBM3 there was a*
825 *significant reduction in HA* ***(A)****, NA* ***(B)*** *and M2* ***(C)*** *mRNA levels, as determined by multiple t-tests. *=p<0.05, **=p<0.01,*
826 ****=p<0.001*

827

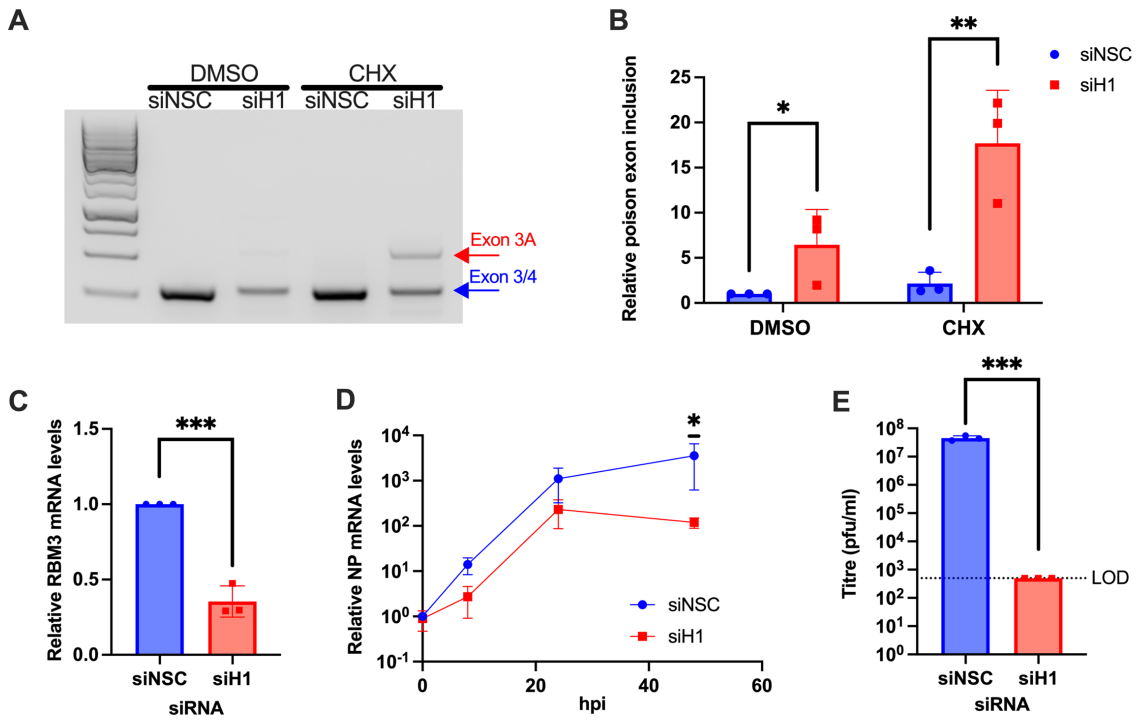

Supplementary Figure 2-Reduced RBM3 levels through manipulation of HNRNPH1 expression suppressed IAV replication

(A) *DNA gel showing inclusion of RBM3's poison exon, exon 3a. Cells were treated with siHNRNPH1 or siNSC and further treated 48 hours post-transfection with DMSO or CHX.* ***(B)*** *qPCR quantification of poison exon inclusion in the samples from Fig. 2D.* ***(C)*** *Quantification of RBM3 mRNA levels in siHNRNPH1 (siH1) A549 cells compared to siNSC treated cells.* ***(D)*** *Transcription levels of NP mRNA in siHNRNPH1 or siNSC treated A549 cells infected with WSN at 37°C. (**E**) Viral titres 72 hpi with WSN MOI 0.01 for siHNRNPH1 or siNSC treated cells.*

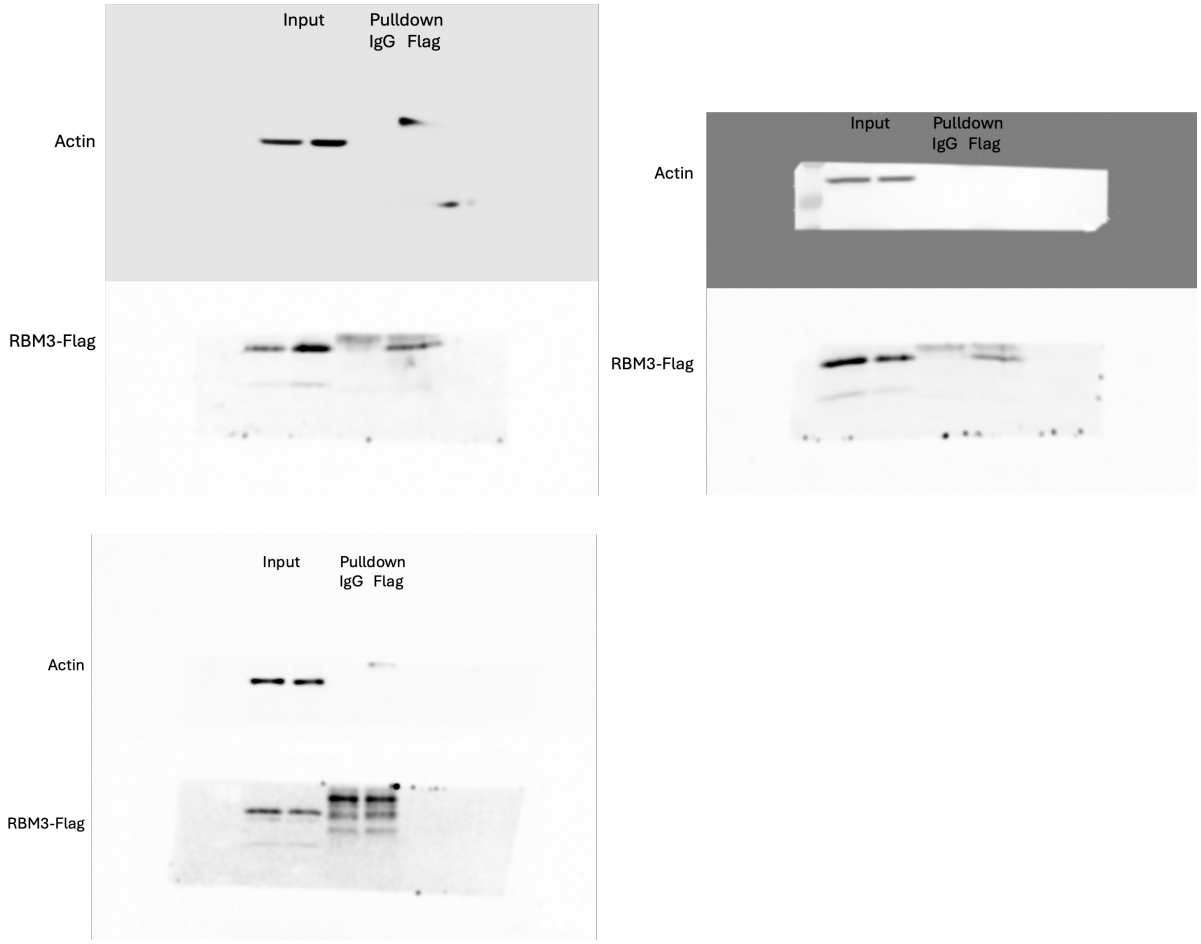

Supplementary Figure 3 – Western blot replicates for CLIP-qPCR in Figure 3E.

3 replicates of CLIP-qPCR experiments to pulldown RBM3-Flag in infected A549 cells demonstrating that RBM3-Flag is present in both input samples but only pulled down in the presence of Flag antibody, while Actin is not enriched in either pulldown sample.